A grain refinement mechanism of cast commercial purity aluminium by vanadium

Feng Wang[1*], Yu-Lung Chiu[1], Dmitry Eskin[2], Wenjia Du[3], Paul R. Shearing[3]

[1]School of Metallurgy and Materials, The University of Birmingham, Edgbaston, B15 2TT, UK

[2]Brunel Centre for Advanced Solidification Technology, Brunel University London, Uxbridge, UB8 3PH, UK

[3]The Electrochemical Innovation Lab, Department of Chemical Engineering, University College London, London, WC1E 7JE, UK

*Corresponding author email: f.wang.4@bham.ac.uk

Abstract: Grain refinement of cast commercial purity aluminium by vanadium and the underlying mechanism have been investigated. Addition of 0.3 wt% and 0.4 wt% vanadium leads to columnar to equiaxed transition and the average grain sizes are refined to around 196 μm and 154 μm, respectively. Pro-peritectic equilibrium $Al_{10}V$ particles are identified near the grain centres. These $Al_{10}V$ particles have either octahedron or plate morphology with the bound planes belonging to {111} crystallographic planes. Three orientation relationships are also determined between the $Al_{10}V$ particles and aluminium grains. Crystallographic analysis based on the experimental orientation relationships indicates that the $Al_{10}V$ particles have relatively high nucleation potency for solid aluminium. Calculation of free growth undercooling based on the size distribution of the $Al_{10}V$ particles reveals that the relatively large size of $Al_{10}V$ particles facilitates the grain initiation of aluminium grains on these particles. Moreover, it is found that the level of vanadium added provides sufficient growth restriction effect in the aluminium melt as quantified by its growth restriction factor. All the three factors, i.e., sufficient potency of $Al_{10}V$ particles, relatively large size of the $Al_{10}V$ particles and adequate growth restriction effect by solute vanadium work in concert to achieve the grain refinement observed in Al-V alloys.

Keywords: grain refinement, aluminium alloys, vanadium, TEM, FIB, crystallography

1. Introduction

Grain refinement is desirable in the commercial production of Al and its alloys because it benefits the casting process, ensures consistent properties of castings, and facilitates the subsequent thermomechanical and other downstream processing [1-7]. In foundries and cast shops, adding grain refiners such as Al-5Ti-1B master alloys prior to pouring is standard practice to obtain grain refinement in the aluminium castings [4-6]. This method of chemical inoculation is simple and effective. The underlying grain refining mechanism has been extensively investigated [3, 8-15]. Although some of the details of the mechanism are under dispute [3, 9-12], it is now generally accepted that these grain refiners contain copious active potent nucleation particles, i.e., TiB_2 particles, to enhance the heterogeneous nucleation of α-Al grains and enough solute element, i.e., Ti solute, to effectively restrict the growth of nucleated α-Al grains, both mechanisms working in concert and leading to effective grain refinement [6, 9-12, 16].

However, these popular Al-5Ti-1B grain refiners are not without problems [5]. One of the notorious issues is that they suffer from a poisoning effect in the Al alloys containing Zr, Cr, Li and high level of Si solute elements [5, 10]. This refers to the phenomenon when the effectiveness of Al-5Ti-1B grain refiners degrades in the Al alloys in the presence of these solute elements due to the formation of compounds that do not possess nucleation potency [17-28]. Consequently, alternative grain refiners are required to achieve reasonable grain refinement in these Al alloys. For example, sub-stoichiometric (the stoichiometric weight ratio of Ti:B in the TiB_2 phase is around 2.2:1) Al-Ti-B master alloys [28-31] and grain refiners based on Al-Ti-C [32-35], Al-Ti-B-C [36-38], Al-B [39-41], and Al-Nb-B [42-44] systems have been developed for the grain refinement of Al alloys containing these alloying elements. Although these newly developed grain refiners have been reported to produce adequate grain refinement, the fundamental ideas behind the design of these new grain refiners are extrapolated from the Al-5Ti-1B grain refiners by changing the nucleation substrates from TiB_2 particles to TiC, AlB_2 or NbB_2 particles. It is also realised that these grain refiners suffer from an inefficiency problem [6]. It is found that as low as only 1% of the added particles do initiate Al grains during solidification while the rest remain inactive and stay in the final

castings [6, 45]. This low efficiency is undesirable not only because it causes extra cost but also because the remaining refiner particles often form agglomerates, being pushed to the grain boundaries, and then act as crack origin under deformation, hence becoming detrimental to the final castings. This is particularly harmful for the products intended for extrusion, deep drawing, and high-performance structural applications.

On the other hand, much less attention has been paid to the long-recognised grain refinement effect associated with the alloying elements forming peritectic systems with Al [2, 46, 47] when considering developing new grain refiners for Al alloys. It is understood that the grain refinement associated with the peritectic Al alloys is closely related to the pro-peritectic particles that crystallises as primary particles during solidification [48]. The reason why the grain refinement associated with the peritectic Al alloys has not attract much attention is probably attributed to the critical fact that the pro-peritectic particles often grow to considerable size under conventional casting conditions, which often involve either slow cooling rates such as sand casting or nearly isothermal holding such as in direct chill (DC) casting, and, hence, act as stress concentrators and crack initiators under deformation, deteriorating the mechanical properties [49, 50]. Nevertheless, under some casting conditions where the cooling rates are relatively high such as upon high pressure die casting and additive manufacturing or with physical melt processing such as ultrasonic melt processing [51] and intensive melt shearing [52, 53], it is believed that the pro-peritectic particles may make contribution to grain refinement of Al alloys without severely deteriorating the mechanical properties. Moreover, from the theoretical point of view, the knowledge obtained from the grain refinement effect with peritectic Al alloys may also be transferable to other metal and alloy systems such as Mg-, Zn-, Ti-, and Ni- alloys. Therefore, a comprehensive understanding of the characteristics of the pro-peritectic particles that can produce grain refinement in Al alloys still bears merits for the development of new effective grain refiners for cast alloys.

The grain refinement effect has been demonstrated in a few peritectic Al alloys [2, 46, 48, 54] and the underlying mechanism is proposed to be attributable to the pro-peritectic

particles that are formed during solidification of the peritectic Al alloys [48, 55, 56]. One of the intriguing peritectic systems is Al-V. However, limited work has been published on the effect of V on grain refinement [46, 48, 57, 58]. It is reported that vanadium addition in the range from 100 ppm to 1000 ppm in aluminium alloys had no observable effect on the grain size [58-62] while the addition of V above 1000 ppm produces adequate grain refinement with increasing V content [46, 48, 57]. Although it is postulated that the grain refinement observed in the Al-V alloys is due to the formation of pro-peritectic particles, the detailed experimental evidence was not provided [48]. Furthermore, it is noticed that there is a cascade of peritectic reactions involving a series of pro-peritectic particles, $Al_{10}V$[63], $Al_{45}V_7$[64], $Al_{23}V_4$[65] and Al_3V[66] on the Al-rich side of the binary phase diagram [67]. According to the equilibrium phase diagram, the peritectic reaction involving the formation of Al solid is at 662.1 °C as follows: $L + Al_{10}V \rightarrow \alpha$-Al. The maximum solubilities of V in liquid and solid at peritectic temperature are 0.17 wt.% and 0.56 wt.%, respectively. This feature raises a question about the identity of the pro-peritectic particles because the formation of pro-peritectic particles is dependent on the casting conditions where fast cooling rates may facilitate the formation of non-equilibrium pro-peritectic particles[68-70]. This may alter the nucleation potency of the particles, limit the operation window of cooling conditions, and affect the grain refinement in the Al-V alloys.

In the present work, the grain refinement effect of peritectic Al-V alloys has been assessed by AA-TP1 test with a cooling rate around 3.5 °C/s which is intended to duplicate the cooling rate found in DC casting [6, 71]. The pro-peritectic particles formed in the as-cast Al-V alloy samples have been characterised in detail by electron microscopy and X-ray microtomography. Furthermore, the mechanism responsible for the grain refinement in peritectic Al-V alloys has been discussed in terms of grain nucleation, grain initiation and grain growth.

2. Experimental

Commercial purity Al (~1.2 kg for each experiment) was melted in the clay-bonded

graphite crucibles inside an electrical resistance furnace and heated up to 720 ºC, at which point an Al-5 wt% V master alloy of prescribed amount was added with manual stirring using a ceramic rod to obtain a series of Al-0.1% V, Al-0.2% V, Al-0.3% V and Al-0.4% V alloys. All alloy compositions are in weight percent unless otherwise stated. After 30 min isothermal holding at 720 ºC, the alloy melt was then cast in the AA TP1 moulds that were pre-heated in an oven at 350 ºC for around 2 hours following the procedure described by the AA TP1 test [72].

The as-cast TP1 samples were then cut along the longitudinal cross sections for composition and macrostructure analysis. The longitudinal cross sections were mechanically ground to 1200 grit SiC paper and etched by Tucker's solution to display the macrostructure. For composition analysis, the longitudinal cross sections were analysed by a Foundry-Master Pro optical emission spectrometer (Oxford Instruments). The nominal chemical compositions and the measured values are listed in Table 1.

Table 1. Nominal and measured chemical compositions of the alloy samples

(All compositions are in weight percent)

Sample No.	Nominal addition	Chemical analysis
Al-0.1%V	0.1%	0.09%
Al-0.2%V	0.2%	0.19%
Al-0.3%V	0.3%	0.31%
Al-0.4%V	0.4%	0.42%

The transvers sections 38 mm from the base of the TP1 samples were also cut and mechanically polished. These samples were then anodized in a 0.5% HBF_4 solution for about 2 min at 15 V DC for microstructure and grain size measurement. The cross sections were examined by optical microscopy (ZEISS Axioscope 5) using polarized light and the grain sizes were measured using a linear intercept technique (ASTM E-112-10). Whenever possible, depending on the grain size, at least five fields of view were examined, and more than 50 counts were obtained on each field.

The samples with considerable grain refinement were investigated in a lab-based X-ray micro-scale CT scanner (ZEISS Xradia 620 Versa) for 3D morphology reconstruction

of the pro-peritectic particles. A polychromatic cone-beam source employing a tungsten target with the voltage set at 80 kV was used with an exposure time of 35 s per projection, and a total of 1401 projection images were collected per scan using 20 × magnification. The 2048×2048 CCD camera detector was used to achieve a voxel resolution at ca. 0. 38 μm with a field of view of 770×770 μm^2. The radiographic projections were then reconstructed using a filtered-back projection algorithm (XMReconstructor). The 3D morphology visualization was carried out in the Avizo software package (Thermo Fisher Scientific, UK).

Furthermore, these samples were then examined in the dual beam microscopes (ZEISS Cross Beam 340 and ThermoFisher Scientific P-FIB) to further investigate the pro-peritectic particles and to prepare the lamella foils for transmission electron microscopy (TEM). TEM was conducted in a JEOL 2100F microscope operated at 200 kV.

3. Results

Figure 1 shows the typical macrostructures of the Al-V alloys studied. The macrostructure changes from fully columnar grains in pure Al to increasing proportions of equiaxed grains and eventually to nearly complete fine equiaxed grains as the vanadium addition level increases. Based on the micrographs shown in Figure 2(a)-2(e), the average grain sizes of the alloy samples were measured and plotted in Figure 2(f). The average grain size experiences substantial refinement even upon adding 0.1% V, from around 1000 μm for pure Al to about 554 μm for the Al-0.1%V alloy. However, it should be noted that the grains are still columnar as can be seen from the macrograph in Figure 1(b). Addition of 0.3%V transforms nearly all the grains into equiaxed grains and decreases the average size to about 196 μm. Further addition of V to the level of 0.4% further refines the grains to an average size of 154 μm.

To determine the factors that are responsible for the grain refinement obtained in the Al-V alloys, the samples with pronounced grain refinement, i.e., the Al-0.3%V and Al-0.4%V, were firstly examined in the dual beam microscope. It is found that distinct particles indicated by red arrows were observed in the samples and many of them were located near grain centres as shown in Figure 3(a) and 3(b). Energy dispersive X-ray

spectroscopy (EDS) analysis on these particles reveals that they are rich in vanadium and the atomic ratio of Al to V is close to 10:1. This implies that these particles could be the pro-peritectic $Al_{10}V$ particles in equilibrium with α-Al according to the phase diagram [67].

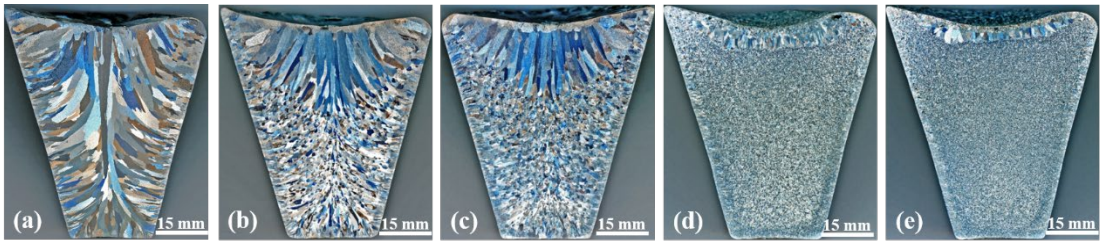

Figure1 Macrostructure of the ac-cast TP1 samples (a) pure Al, (b) Al-0.1%V, (c) Al-0.2%V, (d) Al-0.3%V, and (e) Al-0.4%V

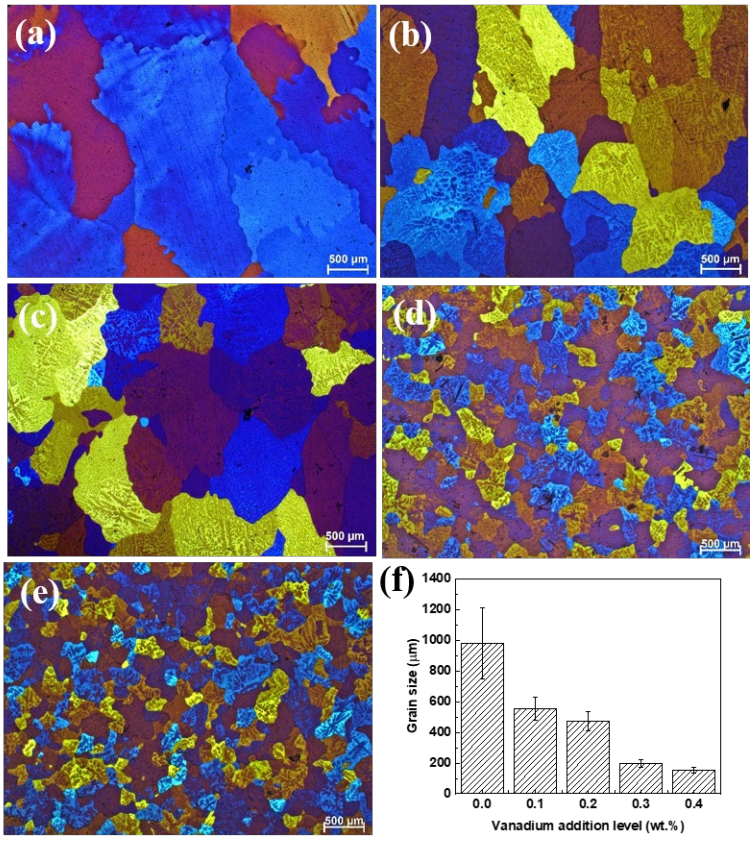

Figure 2 Typical micrographs of the transverse cross sections of the as-cast TP1samples (a) pure Al, (b) Al-0.1%V, (c) Al-0.2%V, (d) Al-0.3%V, (e) Al-0.4%V, and (f) the plot of the average grain size measured based on the micrographs

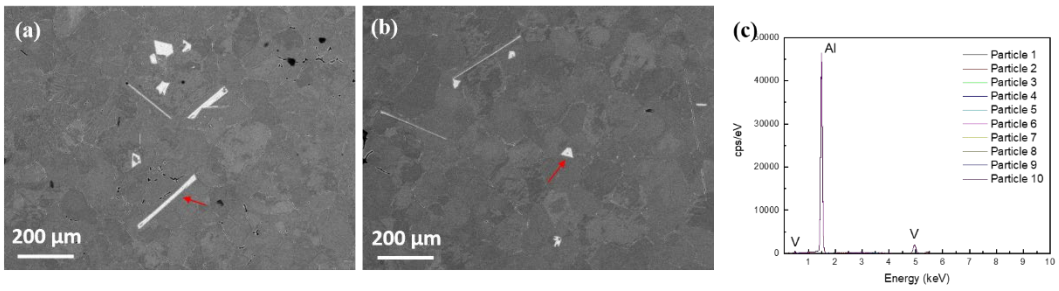

Figure 3 (a) A typical particle observed at the grain centre in the Al-0.3%V sample, (b) A typical particle observed at the grain centre in the Al-0.4%V sample, (c) EDS spectra acquired from ten particles that are the same as the ones in (a) and (b)

Following the observation of the V-rich particles near grain centres, the TEM lamella containing the V-rich particles and the surrounding Al grain matrix were prepared by FIB. In total, ten TEM lamella specimens with thickness around 60 nm were prepared. First, the crystal structure of these V-rich particles was determined by selected area diffraction patterns (SADPs) along a series of tilting angles as represented in Figure 4. It is revealed that all the V-rich particles in the ten TEM foil specimens represent the equilibrium $Al_{10}V$ phase, which has an F.C.C. crystal structure with the lattice parameter a = 1.4492 nm. There are 160 Al atoms and 16 V atoms in the unit cell with space group *Fd3m* [63].

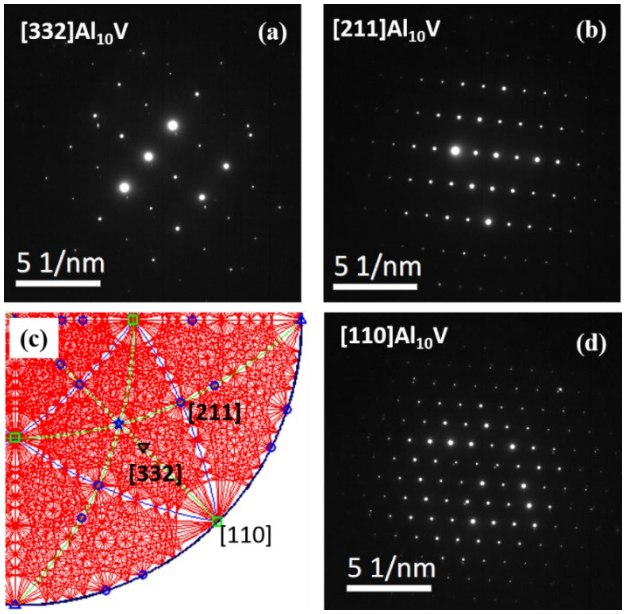

Figure 4 A typical series of SADPs for a V-rich particle at different tilting angles as the beam direction identified along (a) $[332]_{Al10V}$, (b) $[211]_{Al10V}$ and (d) $[110]_{Al10V}$

Moreover, by tilting the exposed habit plane to the edge-on position, HRTEM lattice images of the habit planes have been taken and the *d*-spacing has been measured as represented in Figure 5. It is identified that the exposed habit planes of these $Al_{10}V$ particles belong to {111} crystallographic planes.

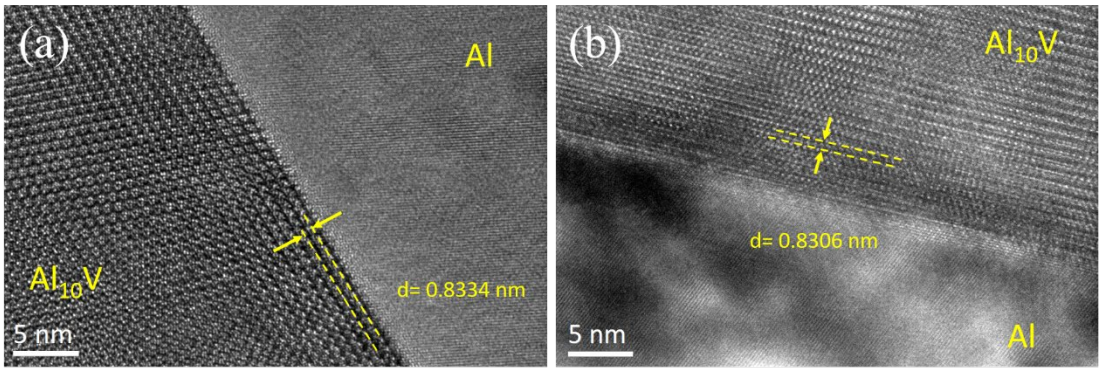

Figure 5 Typical HRTEM lattice images of the exposed habit planes at edge-on position (a) beam direction along $[110]_{Al10V}$ direction and (b) beam direction along $[112]_{Al10V}$ direction

Three different orientation relationships (ORs) have been observed between the $Al_{10}V$ particles and Al grains during the examination of the ten TEM specimens. The HRTEM lattice images of the interface between the $Al_{10}V$ particle and Al grain matrix, the corresponding fast Fourier transforms (FFT), and the simulated overlapped SADPs for the three orientation relationships are shown in Figures 6, 7, and 8, respectively.

As we can see in Figure 6(a), good lattice matching across the interface between the $Al_{10}V$ particle and Al grain matrix has been observed. In addition, the OR can be determined by comparing FFT with the simulated overlapped SADPs. This OR is denoted as OR (I) in the present work and can be represented as:$[10\bar{1}]_{Al}$ //$[11\bar{2}]_{Al10V}$, $(020)_{Al}//(444)_{Al10V}$.

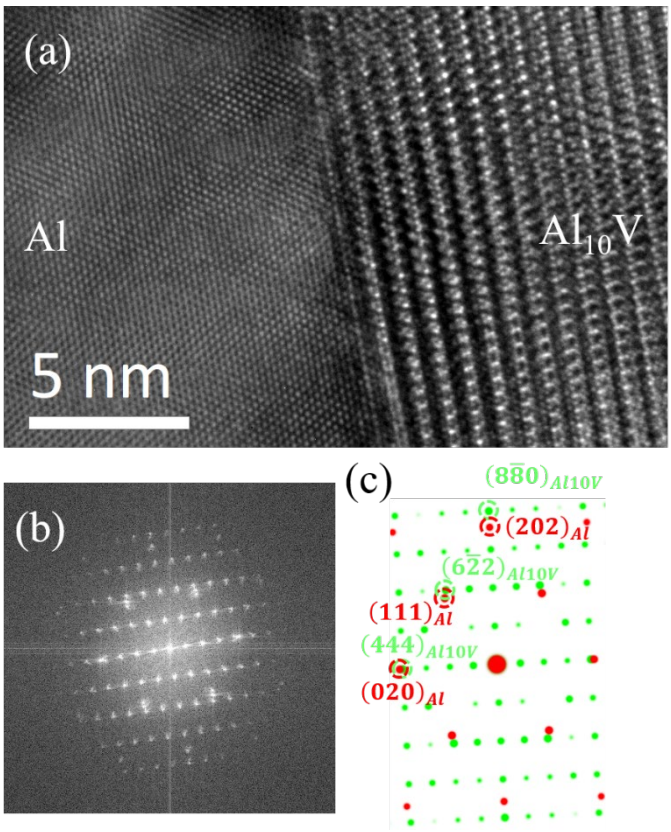

Figure 6 (a) The HRTEM lattice image of the interface between the Al10V particle and Al grain matrix, (b) the corresponding FFT of the lattice image, and (c) the simulated overlapped SADPs red spot pattern for Al and green spot pattern for Al10V for OR(I)

Similarly, the ORs shown in the Figures (7) and (8) are determined and denoted as OR(II) and OR(III) respectively. The OR(II) in Figure 7 can be represented as $[01\bar{1}]_{Al}\,//[12\bar{3}]_{Al10V}$ and $(111)_{Al}//(444)_{Al10V}$ while Figure (8) shows that the OR(III) can be represented as $[10\bar{1}]_{Al}\,//[10\bar{1}]_{Al10V}$ and $(111)_{Al}//(444)_{Al10V}$.

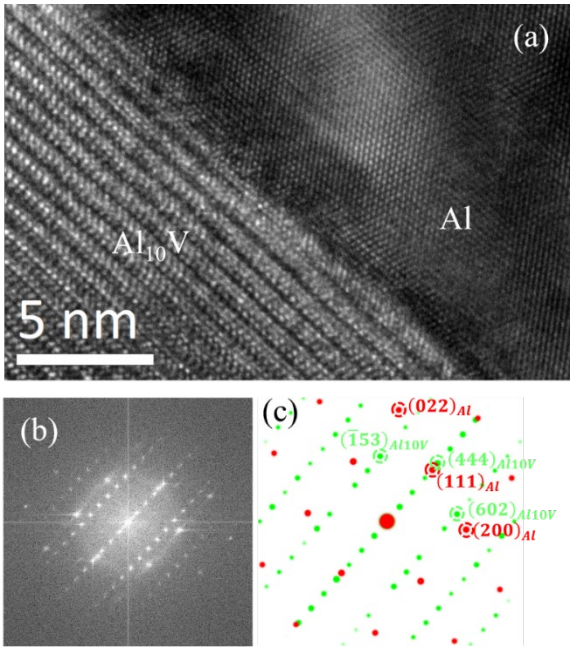

Figure 7 (a) The HRTEM lattice image of the interface between the Al10V particle and Al grain matrix, (b) the corresponding FFT of the lattice image, and (c) the simulated overlapped SADPs red spot pattern for Al and green spot pattern for Al10V for OR(II)

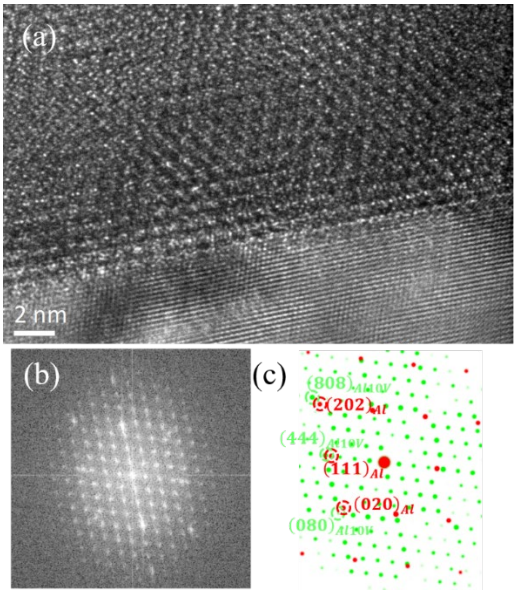

Figure 8 (a) The HRTEM lattice image of the interface between the Al10V particle and Al grain matrix, (b) the corresponding FFT of the lattice image, and (c) the simulated overlapped SADPs: red spot pattern for Al and green spot pattern for Al10V for OR(III)

Besides, the 3D microstructure of Al-0.4%V alloy obtained by micro-CT is illustrated in Figure 9 (only $Al_{10}V$ particles were rendered), revealing two distinct morphologies for the $Al_{10}V$ particles formed in the present work. One is the octahedron morphology as shown in Figure 9(b) and (c). The other one is the plate morphology as shown in Figure 9(d) and (e). On one hand, the octahedron morphology can be easily understood by the fact that the $Al_{10}V$ crystal has a cubic unit cell which has 4 octahedral {111} planes [63] and that the $Al_{10}V$ particles are bound by {111} crystallographic planes as determined by TEM examination (Figure 5).

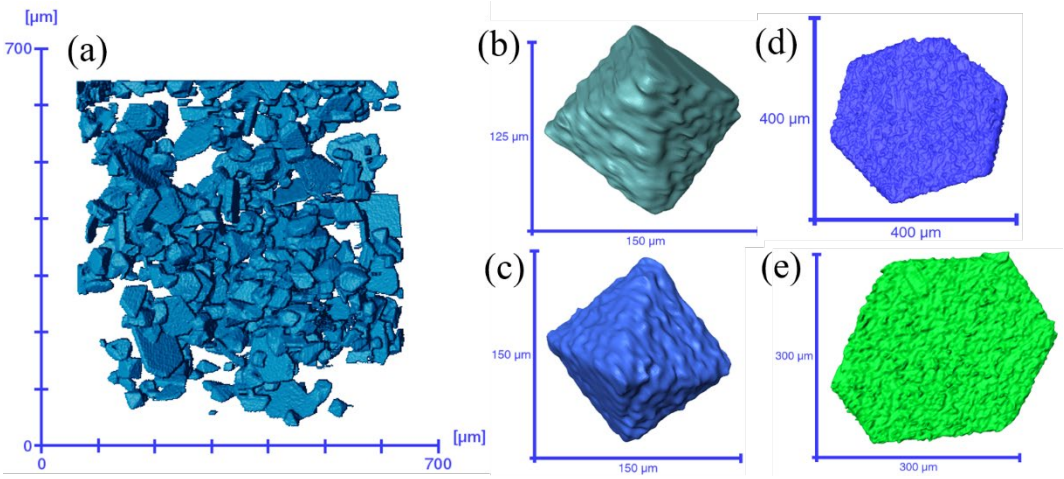

Figure 9 3D microstructure of the $Al_{10}V$ particles formed in the Al-0.4%V alloy sample (a) Overview of the $Al_{10}V$ particles, (b) and (c) typical $Al_{10}V$ particles with octahedron morphology, (d) and (e) typical $Al_{10}V$ particles with plate morphology

On the other hand, the plate morphology is suggested to be caused by the twinning formed during growth of the $Al_{10}V$ particles. The HRTEM image and FFT in Figure 10 clearly shows the presence of twinning in an $Al_{10}V$ particle and hence it is highly possible that the $Al_{10}V$ particles of plate morphology form by twin plane re-entrant edge growth mechanism [73]. More details about the $Al_{10}V$ particles, particularly, the volume fraction and number density per volume, will require further analysis of the reconstructed 3D volume and will be reported in another paper.

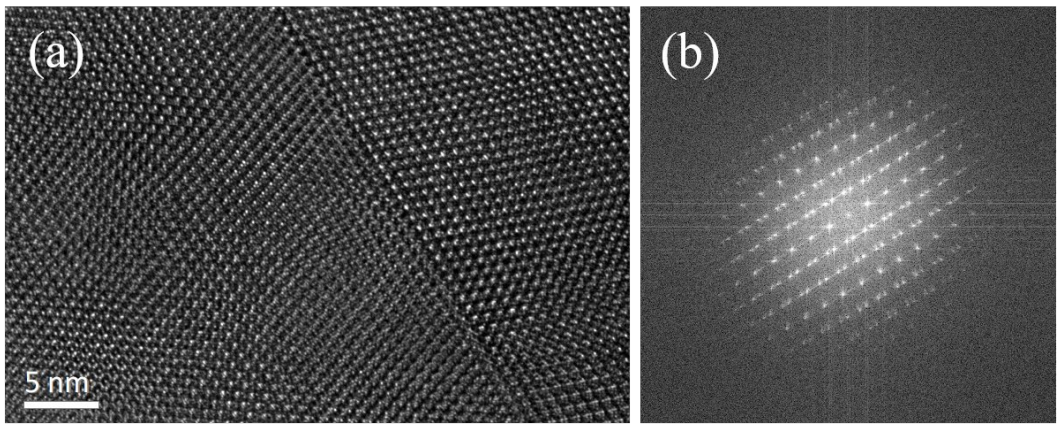

Figure 10 (a) HRTEM lattice image of the twin plane inside an $Al_{10}V$ particle, (b) FFT of (a) showing twinning patterns

4. Discussion

It is widely accepted that the crystallographic matching between the particle and the Al is an important factor to assess the potency of a particle as nucleation site for an Al grain [4, 5, 74] because good crystallographic matching facilitates the heterogeneous nucleation of solid Al on the particle by lowering one of the energy barriers, i.e., the interfacial energy between solid Al and the particle, during heterogeneous nucleation process [4, 5, 50]. Therefore, it is critical to evaluate the crystallographic matching between the $Al_{10}V$ particle and Al grain based on the ORs observed in the experiment. As observed in the TEM examination, the $Al_{10}V$ particles formed in the Al-V alloy samples are bound by {111} crystallographic planes which then act as substrates for the solid Al grain to nucleate on. Consequently, it is important to understand the atomic arrangement of the {111} planes of $Al_{10}V$ crystal.

Based on the unit cells provided in the literature [63], it is found that there are three different types of {111} planes in terms of atomic arrangement as illustrated in Figure 11. Note that the atoms slightly above and below the atomic plane are included in the Type (III) $(111)_{Al10V}$ plane. Moreover, it is also noticed that the crystallographic directions in the planes also have different atomic arrangements. For instance, the$[11\bar{2}]$ direction on the three different (111) planes have three different atomic arrangements which gives three different interatomic spacings. For comparison, the atomic

arrangement on the $\{020\}_{Al}$ and $\{111\}_{Al}$ planes are illustrated in Figure 12.

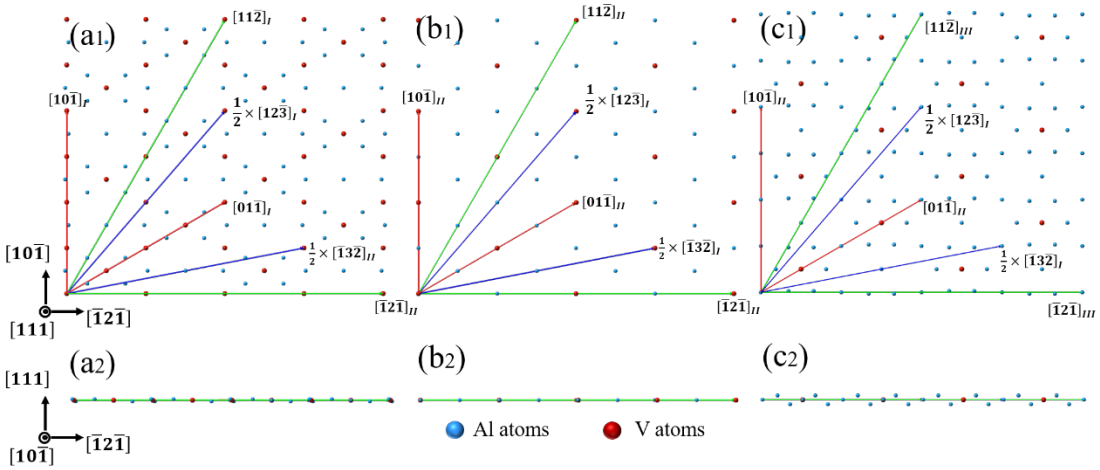

Figure 11 Atomic arrangement on (a1) and (a2): Type (I), (b1) and (b2) Type (II) and (c1) and (c2) Type (III) $(111)_{Al10V}$ plane. Crystallographic directions identified in the experimental ORs are highlighted.

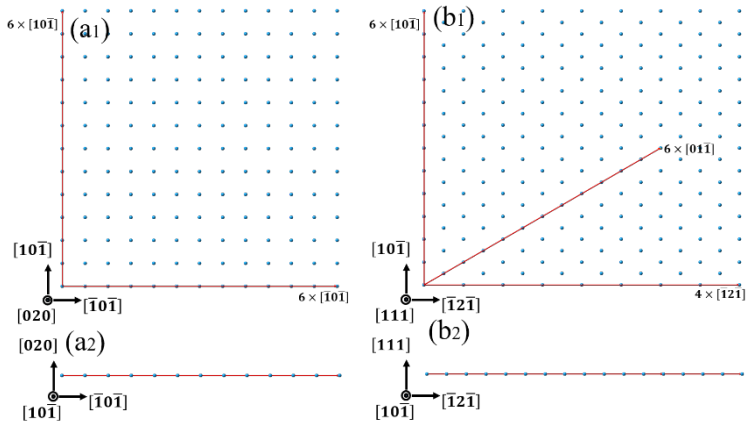

Figure 12 Atomic arrangement on (a1) and (a2): $(020)_{Al}$, and (b1) and (b2): $(111)_{Al}$. Crystallographic directions identified in the experimental ORs are highlighted.

From the atomic arrangements of the crystallographic directions and planes in both Al and $Al_{10}V$ and the ORs determined by experiments, the interatomic spacing misfit, f_r, and interplanar spacing mismatch, f_d, have been calculated according to the following equations [74, 75]:

$$f_r = \frac{|n \times r_{Al} - r_{Al10V}|}{r_{Al10V}} \times 100\%$$

$$f_d = \frac{|d_{Al} - d_{Al10V}|}{d_{Al10V}} \times 100\%$$

where n is a non-zero integer introduced to account for the cases in which two or more interatomic spacings of Al match with one interatomic spacing of $Al_{10}V$; r_{Al} and r_{Al10V} are the interatomic spacings along one direction for Al and $Al_{10}V$, respectively; d_{Al} and d_{Al10V} are the interplanar spacings for Al and $Al_{10}V$, respectively.

The results are listed in Table 2. On one hand, for OR(I), the value of f_d is 3.2% and the value of f_r is 3.15% for Type (II) and Type (III) $[11\bar{2}]_{Al10V}$ direction. These values are much smaller than the critical value of 10% as summarised from the calculations for the common potent grain refiners in Al alloys [74, 75]. On the other hand, the value of f_d for OR(II) and OR(III) is 11.77% while the values of f_r for OR(II) along Type (II) $[12\bar{3}]_{Al10V}$ direction and OR(III) are 15.46% and 11.83% respectively. Both values of f_d and f_r are larger than 10%. In summary, the calculation indicates that the $Al_{10}V$ particles do have reasonably good atomic matching with Al at certain ORs and, hence, strong potency as nucleation site for Al grains from crystallography point of view.

Table 2 The calculated values of f_d and f_r based on experimental ORs

OR(I)					
$d_{(020)Al}$ (nm)	$d_{(444)Al10V}$ (nm)	f_d (%)	$r_{[10\bar{1}]Al}$ (nm)	$r_{[11\bar{2}]Al10V}$ Type (I) (nm)	f_r $\lvert 2 \times r_{Al} - r_{Al10V} \rvert / r_{Al10V}$ (%)
0.2025	0.2092	3.20	0.2865	0.4437	29.13
$d_{(020)Al}$ (nm)	$d_{(444)Al10V}$ (nm)	f_d (%)	$r_{[10\bar{1}]Al}$ (nm)	$r_{[11\bar{2}]Al10V}$ Type (II) (nm)	f_r $\lvert 3 \times r_{Al} - r_{Al10V} \rvert / r_{Al10V}$ (%)
0.2025	0.2092	3.20	0.2865	0.8874	3.15
$d_{(020)Al}$ (nm)	$d_{(444)Al10V}$ (nm)	f_d (%)	$r_{[10\bar{1}]Al}$ (nm)	$r_{[11\bar{2}]Al10V}$ Type (III) (nm)	f_r $\lvert r_{Al} - r_{Al10V} \rvert / r_{Al10V}$ (%)
0.2025	0.2092	3.20	0.2865	0.2958	3.15
OR(II)					

$d\ (111)_{Al}$ (nm)	$d\ (444)_{Al10V}$ (nm)	f_d (%)	$r\ [01\bar{1}]_{Al}$ (nm)	$r\ [12\bar{3}]_{Al10V}$ Type (I) (nm)	fr $\lvert 5 \times r_{Al} - r_{Al10V} \rvert / r_{Al10V}$ (%)
0.2338	0.2092	11.77	0.2865	1.3556	5.67
$d\ (111)_{Al}$ (nm)	$d\ (444)_{Al10V}$ (nm)	f_d (%)	$r\ [01\bar{1}]_{Al}$ (nm)	$r\ [12\bar{3}]_{Al10V}$ Type (II) (nm)	fr $\lvert 2 \times r_{Al} - r_{Al10V} \rvert / r_{Al10V}$ (%)
0.2338	0.2092	11.77	0.2865	0.6778	15.46
OR(III)					
$d\ (111)_{Al}$ (nm)	$d\ (444)_{Al10V}$ (nm)	f_d (%)	$r\ [10\bar{1}]_{Al}$ (nm)	$r\ [10\bar{1}]_{Al10V}$ Type (I) (nm)	fr $\lvert r_{Al} - r_{Al10V} \rvert / r_{Al10V}$ (%)
0.2338	0.2092	11.77	0.2865	0.2562	11.83
$d\ (111)_{Al}$ (nm)	$d\ (444)_{Al10V}$ (nm)	f_d (%)	$r\ [10\bar{1}]_{Al}$ (nm)	$r\ [10\bar{1}]_{Al10V}$ Type (II) (nm)	fr $\lvert 2 \times r_{Al} - r_{Al10V} \rvert / r_{Al10V}$ (%)
0.2338	0.2092	11.77	0.2865	0.5124	11.83

In addition to the crystallographic matching with Al, the size of the $Al_{10}V$ particles is another vital factor affecting grain refinement because the size of the nucleant particles is closely related to the grain initiation process in the free growth model [11, 45, 71, 76]. This is described by the free growth undercooling, ΔT_{fg}, that is calculated based on the particle size using the following equation [11, 45, 71, 76]:

$$\Delta T_{fg} = \frac{4\gamma}{\Delta S_v d}$$

where γ is the interfacial energy between solid and liquid which is 0.158 J/m^{-2} for dilute Al alloys [11]; ΔS_v is the entropy of fusion per unit volume which is 1.11×106 $J/m^3 \cdot K$ for dilute Al alloys [11]; and d is the particle size. The size distributions of $Al_{10}V$ particles in the Al-0.3%V and Al-0.4%V alloy samples have been measured based on the BSE SEM images (Figure 3(a) and 3(b)). The results are plotted in Figure 13(a) and

(b) and, accordingly, the free growth undercoolings are calculated and shown in Figure 13(c) and (d). It is found that most of the $Al_{10}V$ particles in both samples have the size in the range from 20 to 160 μm. More importantly, the calculated free growth undercoolings for most of the $Al_{10}V$ particles are in the range from 0.001 K to 0.06 K which are much smaller values than those calculated for the TiB_2 particles in commercial Al-5Ti-1B master alloys [45, 77]. Moreover, the calculated free growth undercoolings for the $Al_{10}V$ particles are also much smaller than the typical value of maximum undercooling, ~0.2 K, measured by cooling curves at recalescence point in Al alloys under comparable cooling rates [11, 71]. This simple comparison implies that the grain initiation was not the rate-controlling process during the solidification and, hence, the relatively large size of the $Al_{10}V$ particles facilitates the grain initiation process and, thereby, grain refinement.

It is important to mention that the distribution of the $Al_{10}V$ particles is not completely uniform across the TP1 ingots and some considerably big $Al_{10}V$ particles are present. The presence of these particles would inevitably affect the mechanical properties as mentioned in the introduction section, in particularly in the production of Al thin foils. Therefore, approaches either by casting with higher cooling rate or by physical melt processing may be required to further improve the distribution of the $Al_{10}V$ particles and to reduce their size. Moreover, the binary peritectic alloy systems have been known for the difficulty of casting due to the high liquidus temperatures. This difficulty would induce solidification porosity and hence affect the mechanical properties. Consequently, it should take extra care regarding the castability of peritectic alloys.

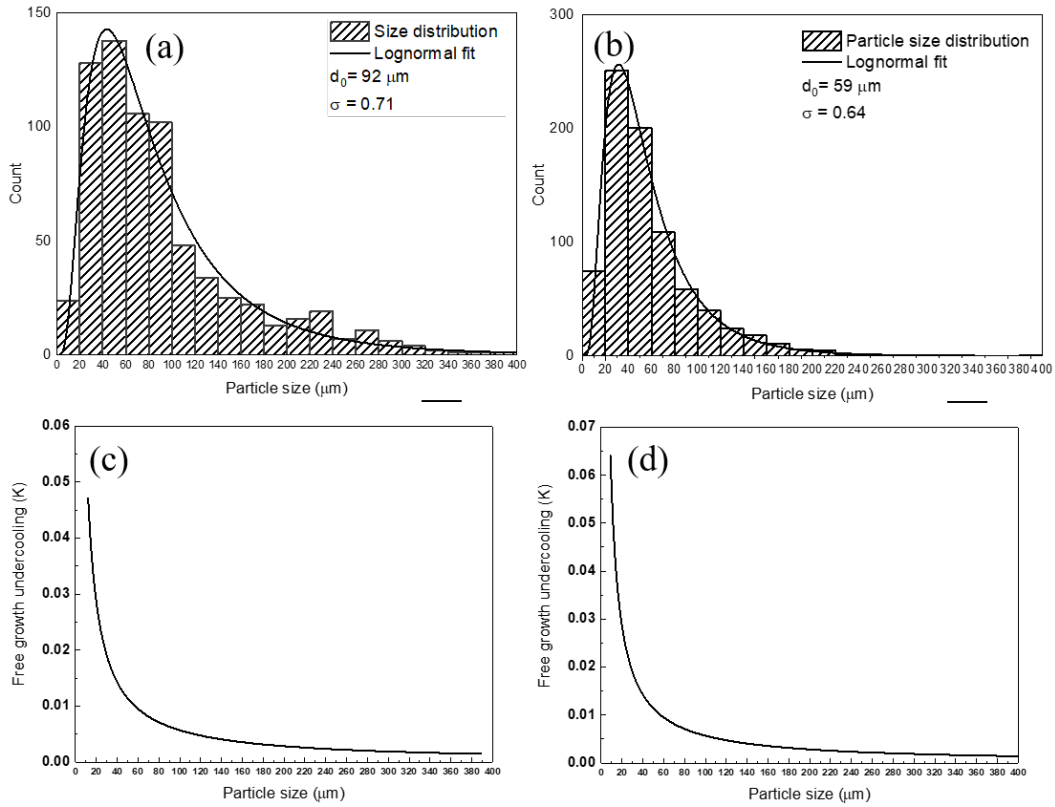

Figure 13 (a) and (b) are the size distributions of the $Al_{10}V$ particles in Al-0.3%V and Al-0.4%V alloy samples, respectively; (c) and (d) are the free growth undercoolings for the $Al_{10}V$ particles in Al-0.3%V and Al-0.4%V alloy samples, respectively

As it is well documented in the literature [3-5, 9, 16], the growth restriction effect and the constitutional undercooling induced by the partitioning of solute elements ahead of the growing solid Al grains also make crucial contribution to effective grain refinement. This is normally quantified by the growth restriction factor, $Q = m_l \cdot (k-1) \cdot c_0$ where m_l is the liquidus slope in the phase diagram of solute with aluminium and is normally approximated to be straight, $k = c_s/c_l$ is the equilibrium partition coefficient, and c_0 is the solute content in the alloy melt [78, 79]. The parameters can be extracted from the binary Al-V equilibrium phase diagram [67] by assuming that the liquidus and solidus lines for α-Al are straight. It is obtained that m_l = 9.71 K/wt% and k = 3.29, resulting in $m_l \cdot (k\text{-}1)$ = 22.24 K/wt%. It is also necessary to point out that, when the solute content in the alloy melt exceeds the maximum liquid solubility, the primary $Al_{10}V$ particles form which reduces the solute content in the alloy melt. Consequently, when calculating the Q value for the solute content larger than the maximum liquid solubility, the c_0 is

replaced by c_m which is the maximum liquid solubility of V in liquid aluminium at the peritectic temperature. This assumes that all the excess solute above the maximum solubility is combined with Al to form $Al_{10}V$ particles according to equilibrium phase diagram. It is important to point out that the pro-peritectic particles identified in the present work are the equilibrium $Al_{10}V$ particles which implies that, under the TP1 casting condition, the Al-V alloys solidified close to equilibrium solidification and that the cooling rate of ~3.5 K/s is not high enough to promote the formation of non-equilibrium pro-peritectic particles in the present work. Therefore, the above assumption is reasonable. The parameter of c_m is also extracted from the phase diagram as 0.17 wt%. Based on these parameters, the Q values for the alloys in the present work are hence 2.2 K (for Al-0.1%V), 3.8 K (for Al-0.2%V), 3.8 K (for Al-0.3%V) and 3.8 K (for Al-0.4%V), respectively. These Q values are comparable to the Q values calculated for the common addition levels of Al-5Ti-1B master alloys (1 to 10 parts per thousand [6, 10]) in commercial-purity aluminium alloys [11, 45, 78] and therefore the V addition levels in the present work can be considered as being sufficient to promote effective growth restriction in the presence of potent $Al_{10}V$ pro-peritectic particles.

5. Conclusions

In the current work, the grain refining effect of V solute content on commercial purity aluminium alloys has been examined. The mechanism underlying the grain refinement has also been investigated with focus on the role of pro-peritectic particles formed during solidification in enhancing grain nucleation and facilitating grain initiation processes. In particular, the identity, habit plane, OR with Al grains, size distribution and 3D morphology of the pro-peritectic particles have been characterised. In summary, the following conclusions have been obtained:

1. Addition of increasing V solute content does induce columnar to equiaxed transition in commercial purity aluminium alloys and the grains with addition of 0.4% V are refined to an average size of about 154 μm.
2. Primary equilibrium $Al_{10}V$ intermetallic particles have been identified in the Al grains. They are bound by {111} crystallographic planes and have either octahedron or plate

morphology. Most of the $Al_{10}V$ particles have the size in the range of 20 to 160 μm under the casting condition in the present work. In addition, twinning has been observed in some of the $Al_{10}V$ particles.

3. Three orientation relationships have been determined between the $Al_{10}V$ particles and Al grains. They are:

   OR(I): $[10\bar{1}]_{Al}$ //$[11\bar{2}]_{Al10V}$, $(020)_{Al}$//$(444)_{Al10V}$;

   OR(II): $[01\bar{1}]_{Al}$ //$[12\bar{3}]_{Al10V}$, $(111)_{Al}$//$(444)_{Al10V}$;

   OR(III): $[10\bar{1}]_{Al}$ //$[10\bar{1}]_{Al10V}$, $(111)_{Al}$//$(444)_{Al10V}$.

4. The evaluation of interatomic spacing misfit and interplanar spacing mismatch reveals that the $Al_{10}V$ particles have relatively good potency as nucleation substrate for Al grains. Moreover, the calculation of free growth undercooling indicates that grain initiation is facilitated by the relatively large particle size of the Al10V particles. Furthermore, the quantification of growth restriction effect by Q values for the Al-V alloys also implies that the V content is sufficient to promote effective grain refinement in the present work.

5. All the three factors, i.e., sufficiently potent $Al_{10}V$ nucleant particles, relatively large size of the $Al_{10}V$ nucleant particles and adequate growth restriction effect by solute vanadium work in concert to achieve the effective grain refinement observed in the peritectic Al-V alloys. This effect should be applicable to a wide range of casting processes with cooling rates around 3.5 K/s and lower (from sand and gravity casting to DC casting).

Acknowledgements

The authors acknowledge the financial support from UK government's Engineering and Physical Science Research Council (EPSRC) (EP/L019884/1). The authors are also grateful to Dr Biao Cai and Mr Zihan Song for their help with access to Avizo software package. P.R.S acknowledges funding from The Royal Academy of Engineering (CiET1718/59).

Data availability

The raw/processed data required to reproduce these findings cannot be shared at this time

as the data also forms part of an ongoing study.

References

[1] A. Cibula, The grain refinement of aluminium alloy castings by additions of titanium and boron, Journal of the Institute of Metals, 80 (1951) 1-16.

[2] F.A. Crossley, L.F. Mondolfo, Mechanism of grain refinement in aluminum alloys, Transactions of the American Institute of Mining and Metallurgical Engineers, 191 (1951) 1143-1148.

[3] M. Easton, D. Stjohn, Grain refinement of aluminum alloys: Part I. The nucleant and solute paradigms - a review of the literature, Metall. Mater. Trans. A, 30 (1999) 1613-1623.

[4] D.G. McCartney, Grain refining of aluminium and its alloys using inoculants, Int. Mater. Rev., 34 (1989) 247-260.

[5] B.S. Murty, S.A. Kori, M. Chakraborty, Grain refinement of aluminium and its alloys by heterogeneous nucleation and alloying, Int. Mater. Rev., 47 (2002) 3-29.

[6] A.L. Greer, P.S. Cooper, M.W. Meredith, W. Schneider, P. Schumacher, J.A. Spittle, A. Tronche, Grain refinement of aluminium alloys by inoculation, Adv. Eng. Mater., 5 (2003) 81-91.

[7] M.A. Easton, M. Qian, A. Prasad, D.H. StJohn, Recent advances in grain refinement of light metals and alloys, Curr. Opin. Solid State Mater. Sci., 20 (2016) 13-24.

[8] P.S. Mohanty, J.E. Gruzleski, Mechanism of grain refinement in aluminium, Acta Metallurgica et Materialia, 43 (1995) 2001-2012.

[9] M. Easton, D. StJohn, Grain refinement of aluminum alloys: Part II. Confirmation of, and a mechanism for, the solute paradigm, Metall. Mater. Trans. A, 30 (1999) 1625-1633.

[10] T.E. Quested, Understanding mechanisms of grain refinement of aluminium alloys by inoculation, Mater. Sci. Technol., 20 (2004) 1357-1369.

[11] T.E. Quested, A.L. Greer, Grain refinement of Al alloys: Mechanisms determining as-cast grain size in directional solidification, Acta Mater., 53 (2005) 4643-4653.

[12] Z. Fan, Y. Wang, Y. Zhang, T. Qin, X.R. Zhou, G.E. Thompson, T. Pennycook, T. Hashimoto, Grain refining mechanism in the Al/Al-Ti-B system, Acta Mater., 84 (2015) 292-304.

[13] Q. Du, Y. Li, An extension of the Kampmann–Wagner numerical model towards as-cast grain size prediction of multicomponent aluminum alloys, Acta Mater., 71 (2014) 380-389.

[14] Y. Xu, D. Casari, Q. Du, R.H. Mathiesen, L. Arnberg, Y. Li, Heterogeneous nucleation and grain growth of inoculated aluminium alloys: An integrated study by in-situ X-radiography and numerical modelling, Acta Mater., 140 (2017) 224-239.

[15] Y. Xu, D. Casari, R.H. Mathiesen, Y. Li, Revealing the heterogeneous nucleation behavior of equiaxed grains of inoculated Al alloys during directional solidification, Acta Mater., 149 (2018) 312-325.

[16] T.E. Quested, A.L. Greer, Growth-restriction effects in grain refinement of aluminium, in: Light Metals 2003: Proceedings of the technical sessions presented by the TMS Aluminium Committee at the 132nd TMS Annual Meetings, March 2, 2003 - March 6, 2003, Minerals, Metals and Materials Society, San Diego, CA, United states, 2003, pp. 945-952.

[17] S.M. Ahmady, D.G. McCartney, S.R. Thistlethwaite, Assessment of aluminum grain refiner performance using the Alcoa Test, in: Light Metals 1990, 1990, pp. 837-843.

[18] M.E.J. Birch, GRAIN REFINING OF ALUMINIUM-LITHIUM BASED ALLOYS WITH TITANIUM BORON ALUMINIUM, in, 1986, pp. 152-158.

[19] J.A. Spittle, S. Sadli, The influence of zirconium and chromium on the grain refining efficiency of Al-Ti-B inoculants, Cast Met., 7 (1995) 247-253.

[20] A. Arjuna Rao, B.S. Murty, M. Chakraborty, Role of zirconium and impurities in grain refinement of aluminium with Al-Ti-B, Mater. Sci. Technol., 13 (1997) 769-777.

[21] M. Johnsson, Influence of Zr on the Grain Refinement of Aluminium, Z. Metallkd., 85 (1994) 786-789.

[22] A. Arjuna Rao, B.S. Murty, M. Chakraborty, Influence of chromium and impurities on the grain-refining behavior of aluminum, Metall. Mater. Trans. A, 27 (1996) 791-800.

[23] C.R. Chakravorty, M. Chakraborty, Grain refining of aluminium-lithium alloy with Al-Ti-B, Cast Met., 4 (1991) 98-100.

[24] J.A. Spittle, Grain refinement in shape casting of aluminium alloys, Int. J. Cast Met. Res., 19 (2006) 210-222.

[25] M. Johnsson, Influence of Zr on the grain refinement of aluminium, Z. Metallk., 85 (1994) 786-789.

[26] M. Johnsson, Influence of Si and Fe on the grain refinement of aluminium, Z. Metallk., 85 (1994) 781-785.

[27] M. Johnsson, L. Bäckerud, The influence of composition on equiaxed crystal growth mechanisms and grain size in Al alloys, Zeitschrift fuer Metallkunde/Materials Research and Advanced Techniques, 87 (1996) 216-220.

[28] G.K. Sigworth, M.M. Guzowski, Grain refining of hypoeutectic Al-Si alloys, in: 89. AFS annual meeting (Pittsburgh, PA 1986), Fachverlag Schiele und Schön GmbH, Berlin, 1987, pp. 51-58.

[29] G.S.V. Kumar, B.S. Murty, M. Chakraborty, Grain refinement response of LM25 alloy towards Al-Ti-C and Al-Ti-B grain refiners, J. Alloys Compd., 472 (2009) 112-120.

[30] Y. Birol, Performance of AlTi5B1, AlTi3B3 and AlB3 master alloys in refining grain structure of aluminium foundry alloys, Mater. Sci. Technol., 28 (2012) 481-486.

[31] S.A. Kori, B.S. Murty, M. Chakraborty, Development of an efficient grain refiner for Al-7Si alloy and its modification with strontium, Mater. Sci. Eng., A, 283 (2000) 94-104.

[32] Y. Birol, Grain refining efficiency of Al-Ti-C alloys, J. Alloys Compd., 422 (2006) 128-131.

[33] P.S. Mohanty, J.E. Gruzleski, Grain refinement mechanisms of hypoeutectic Al-Si alloys, Acta Mater., 44 (1996) 3749-3760.

[34] G.S. Vinod Kumar, B.S. Murty, M. Chakraborty, Development of Al-Ti-C grain refiners and study of their grain refining efficiency on Al and Al-7Si alloy, J. Alloys Compd., 396 (2005) 143-150.

[35] H. Ding, X. Liu, L. Yu, Influence of zirconium on grain refining efficiency of Al-Ti-C master alloys, Journal of Materials Science, 42 (2007) 9817-9821.

[36] P. Li, S. Liu, L. Zhang, X. Liu, Grain refinement of A356 alloy by Al-Ti-B-C master alloy and its effect on mechanical properties, Mater. Des., 47 (2013) 522-528.

[37] J. Nie, X. Ma, H. Ding, X. Liu, Microstructure and grain refining performance of a new Al-Ti-C-B master alloy, J. Alloys Compd., 486 (2009) 185-190.

[38] J. Nie, X. Ma, P. Li, X. Liu, Effect of B/C ratio on the microstructure and grain refining efficiency of Al-Ti-C-B master alloy, J. Alloys Compd., 509 (2011) 1119-1123.

[39] Y. Birol, AlB 3 master alloy to grain refine AlSi10Mg and AlSi12Cu aluminium foundry alloys, J. Alloys Compd., 513 (2012) 150-153.

[40] Y. Birol, Grain refinement of pure aluminium and Al-7Si with Al-3B master alloy, Mater. Sci. Technol., 28 (2012) 363-367.

[41] Z. Chen, H. Kang, G. Fan, J. Li, Y. Lu, J. Jie, Y. Zhang, T. Li, X. Jian, T. Wang, Grain refinement of hypoeutectic Al-Si alloys with B, Acta Mater., 120 (2016) 168-178.

[42] M. Nowak, L. Bolzoni, N. Hari Babu, Grain refinement of Al–Si alloys by Nb–B inoculation. Part I: Concept development and effect on binary alloys, Materials & Design (1980-2015), 66 (2015) 366-375.

[43] L. Bolzoni, M. Nowak, N. Hari Babu, Grain refinement of Al–Si alloys by Nb–B inoculation. Part II: Application to commercial alloys, Materials & Design (1980-2015), 66 (2015) 376-383.

[44] L. Bolzoni, N. Hari Babu, Efficacy of Borides in Grain Refining Al-Si Alloys, Metall. Mater. Trans. A, 50 (2019) 746-756.

[45] T.E. Quested, A.L. Greer, The effect of the size distribution of inoculant particles on as-cast grain size in aluminium alloys, Acta Mater., 52 (2004) 3859-3868.

[46] M.D. Eborall, GRAIN REFINEMENT OF ALUMINIUM AND ITS ALLOYS BY SMALL ADDITIONS OF OTHER ELEMENTS, Journal of the Institute of Metals, 76 (1949) 295-320.

[47] A.A. Abdel-Hamid, Effect of other elements on the grain refinement of Al by Ti or Ti and B. Part II. Effect of the refractory metals V, Mo Zr and Ta, Zeitschrift fuer Metallkunde/Materials Research and Advanced Techniques, 80 (1989) 643-647.

[48] F. Wang, Z. Liu, D. Qiu, J.A. Taylor, M.A. Easton, M.-X. Zhang, Revisiting the role of peritectics in grain refinement of Al alloys, Acta Mater., 61 (2013) 360-370.

[49] W. Kurz, D.J. Fisher, Fundamentals of solidification, 4th rev. ed., Trans Tech Publications, Zurich, Switzerland, 1998.

[50] J.A. Dantzig, M. Rappaz, Solidfication, 2nd ed., EPFL Press, Switzerland, 2016.

[51] D.G. Eskin, I. Tzanakis, F. Wang, G.S.B. Lebon, T. Subroto, K. Pericleous, J. Mi, Fundamental studies of ultrasonic melt processing, Ultrason. Sonochem., 52 (2019) 455-467.

[52] Z. Fan, Y. Wang, M. Xia, S. Arumuganathar, Enhanced heterogeneous nucleation in AZ91D alloy by intensive melt shearing, Acta Mater., 57 (2009) 4891-4901.

[53] Z. Fan, G. Liu, Solidification behaviour of AZ91D alloy under intensive forced convection in the RDC process, Acta Mater., 53 (2005) 4345-4357.

[54] F.R. Morral, F.A. Crossley, L.F. Mondolfo, M.E. Eborall, A. Cibula, W.R. Opie, H. Bernstein, J. Morgan, P.G. England, D. Turnbull, MECHANISM OF GRAIN REFINEMENT IN ALUMINUM ALLOYS - DISCUSSION, Transactions of the American Institute of Mining and Metallurgical Engineers, 194 (1952) 1190-1195.

[55] F. Wang, D. Qiu, Z.-L. Liu, J.A. Taylor, M.A. Easton, M.-X. Zhang, The grain refinement mechanism of cast aluminium by zirconium, Acta Mater., 61 (2013) 5636-5645.

[56] F. Wang, D. Qiu, Z.-L. Liu, J.A. Taylor, M.A. Easton, M.-X. Zhang, Crystallographic study of grain refinement of Al by Nb addition, J. Appl. Crystallogr., 47 (2014) 770-779.

[57] L.F. Mondolfo, Al–V Aluminum–Vanadium system, in: L.F. Mondolfo (Ed.) Aluminum Alloys, Butterworth-Heinemann, 1976, pp. 392-394.

[58] A. Johanson, Effect of Vanadium on Grain Refinement of Aluminium, in: Materials Science and Engineering, Norwegian University of Science and Technology, Trondheim, 2013, pp. 78.

[59] J.F. Grandfield, J.A. Taylor, The Impact of Rising Ni and V Impurity Levels in Smelter Grade Aluminium and Potential Control Strategies, Mater. Sci. Forum, 630 (2010) 129-136.

[60] J. Grandfield, L. Sweet, C. Davidson, J. Mitchell, A. Beer, S. Zhu, X. Chen, M. Easton, An Initial Assessment of the Effects of Increased Ni and V Content in A356 and AA6063 Alloys, in: Light Metals 2013, 2013, pp. 39-45.

[61] J. Grandfield, L. Sweet, A. Beer, S. Zhu, X. Chen, M. Easton, The Effect of Trace Levels of Ni and V on the Microstructure and Properties of Four Common Aluminum Alloys, in: Light Metals 2014, 2014, pp. 969-974.

[62] S. Boczkal, M. Lech-Grega, J. Morgiel, K. Piela, Effect of Vanadium Additions on the

Structure of Aluminium (AL99.5) And 6XXX Aluminium Alloys, in: J. Grandfield (Ed.) Light Metals 2014, Springer International Publishing, Cham, 2016, pp. 261-264.
[63] P. Brown, The structure of alpha-(V-Al), Acta Crystallogr., 10 (1957) 133-135.
[64] P. Brown, The structure of the intermetallic phase alpha'-(VAl), Acta Crystallogr., 12 (1959) 995-1002.
[65] J.F. Smith, A.E. Ray, The structure of V_4Al_{23}, Acta Crystallogr., 10 (1957) 169-172.
[66] G. Brauer, Konstitution der Aluminium-Vanadin-Verbindung VAl3, Zeitschrift für Elektrochemie und angewandte physikalische Chemie, 49 (1943) 208-210.
[67] J.L. Murray, Al-V (aluminum-vanadium), Bulletin of Alloy Phase Diagrams, 10 (1989) 351-357.
[68] Y.J. Bi, M.H. Loretto, Influence of iron impurity on the decomposition behaviour of RSP Al-V solid solutions, International journal of rapid solidification, 5 (1990) 163-175.
[69] X.D. Zhang, M.H. Loretto, Precipitation in melt-spun al-based binary alloys with transition metals, Philosophical Magazine B: Physics of Condensed Matter; Statistical Mechanics, Electronic, Optical and Magnetic Properties, 64 (1991) 697-708.
[70] X.D. Zhang, M.H. Loretto, Stability and decomposition mechanisms of supersaturated solid solutions in rapidly solidified aluminium-transition metal alloys, Mater. Sci. Technol., 12 (1996) 19-24.
[71] A.L. Greer, A.M. Bunn, A. Tronche, P.V. Evans, D.J. Bristow, Modelling of inoculation of metallic melts: application to grain refinement of aluminium by Al-Ti-B, Acta Mater., 48 (2000) 2823-2835.
[72] T.A. Association, Standard Test Procedure for Aluminum Alloy Grain Refiners, Washington D.C., 1990
[73] J.W. Faust, H.F. John, The growth of semiconductor crystals from solution using the twin-plane reentrant-edge mechanism, J. Phys. Chem. Solids, 25 (1964) 1407-1415.
[74] M.X. Zhang, P.M. Kelly, M.A. Easton, J.A. Taylor, Crystallographic study of grain refinement in aluminum alloys using the edge-to-edge matching model, Acta Mater., 53 (2005) 1427-1438.
[75] D. Qiu, J.A. Taylor, M.X. Zhang, Understanding the Co-poisoning Effect of Zr and Ti

on the Grain Refinement of Cast Aluminum Alloys, Metallurgical and Materials Transactions A (Physical Metallurgy and Materials Science), 41 (2010) 3412-3421.

[76] A.L. Greer, T.E. Quested, Heterogeneous grain initiation in solidification, Philos. Mag., 86 (2006) 3665-3680.

[77] T.E. Quested, A.L. Greer, P.S. Cooper, The variable potency of TiB_2 nucleant particles in the grain refinement of aluminium by Al-Ti-B additions, in: Mater. Sci. Forum, 2002, pp. 53-58.

[78] T.E. Quested, A.T. Dinsdale, A.L. Greer, Thermodynamic modelling of growth-restriction effects in aluminium alloys, Acta Mater., 53 (2005) 1323-1334.

[79] R. Schmid-Fetzer, A. Kozlov, Thermodynamic aspects of grain growth restriction in multicomponent alloy solidification, Acta Mater., 59 (2011) 6133-6144.